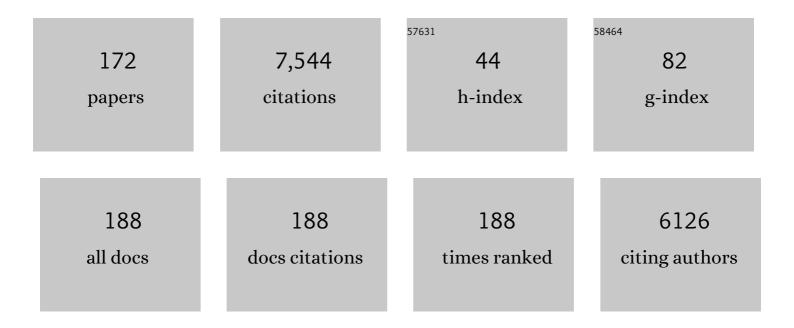
## **Gerhard Glatting**

List of Publications by Year in descending order

Source: https://exaly.com/author-pdf/1396928/publications.pdf Version: 2024-02-01



#	Article	IF	CITATIONS
1	Radiation exposure of patients undergoing whole-body dual-modality 18F-FDG PET/CT examinations. Journal of Nuclear Medicine, 2005, 46, 608-13.	2.8	298
2	Imaging proliferation in lung tumors with PET: 18F-FLT versus 18F-FDG. Journal of Nuclear Medicine, 2003, 44, 1426-31.	2.8	281
3	FDG uptake in breast cancer: correlation with biological and clinical prognostic parameters. European Journal of Nuclear Medicine and Molecular Imaging, 2002, 29, 1317-1323.	3.3	274
4	Early Detection and Accurate Description of Extent of Metastatic Bone Disease in Breast Cancer With Fluoride Ion and Positron Emission Tomography. Journal of Clinical Oncology, 1999, 17, 2381-2381.	0.8	266
5	Fluorine-18 2-deoxy-2-fluoro-D-glucose PET in the preoperative staging of breast cancer: comparison with the standard staging procedures. European Journal of Nuclear Medicine and Molecular Imaging, 2001, 28, 351-358.	2.2	225
6	2-(fluorine-18)fluoro-2-deoxy-D-glucose positron emission tomography in the detection and staging of malignant lymphoma. Cancer, 2001, 91, 889-899.	2.0	221
7	EANM Dosimetry Committee guidelines for bone marrow and whole-body dosimetry. European Journal of Nuclear Medicine and Molecular Imaging, 2010, 37, 1238-1250.	3.3	217
8	Chronic osteomyelitis: detection with FDG PET and correlation with histopathologic findings Radiology, 1998, 206, 749-754.	3.6	200
9	Choosing the optimal fit function: Comparison of the Akaike information criterion and the Fâ€ŧest. Medical Physics, 2007, 34, 4285-4292.	1.6	193
10	Imaging prostate cancer with 11C-choline PET/CT. Journal of Nuclear Medicine, 2006, 47, 1249-54.	2.8	191
11	Molecular Imaging of Proliferation in Malignant Lymphoma. Cancer Research, 2006, 66, 11055-11061.	0.4	173
12	[11C]choline PET/CT imaging in occult local relapse of prostate cancer after radical prostatectomy. European Journal of Nuclear Medicine and Molecular Imaging, 2008, 35, 9-17.	3.3	168
13	Rhenium 188–labeled anti-CD66 (a, b, c, e) monoclonal antibody to intensify the conditioning regimen prior to stem cell transplantation for patients with high-risk acute myeloid leukemia or myelodysplastic syndrome: results of a phase I-II study. Blood, 2001, 98, 565-572.	0.6	166
14	3-deoxy-3-[(18)F]fluorothymidine-positron emission tomography for noninvasive assessment of proliferation in pulmonary nodules. Cancer Research, 2002, 62, 3331-4.	0.4	162
15	F-18 NaF PET for Detection of Bone Metastases in Lung Cancer: Accuracy, Cost-Effectiveness, and Impact on Patient Management. Journal of Bone and Mineral Research, 2003, 18, 2206-2214.	3.1	155
16	Values and Limitations of 18F-Fluorodeoxyglucose???Positron-Emission Tomography with Preoperative Evaluation of Patients with Pancreatic Masses. Pancreas, 2000, 20, 109-116.	0.5	151
17	2-(fluorine-18)-fluoro-2-deoxy-D-glucose PET in detection of pancreatic cancer: value of quantitative image interpretation Radiology, 1995, 195, 339-344.	3.6	149
18	Second cancer risk after 3D-CRT, IMRT and VMAT for breast cancer. Radiotherapy and Oncology, 2014, 110. 471-476.	0.3	138

#	Article	IF	CITATIONS
19	A multicentre comparison of quantitative 90Y PET/CT for dosimetric purposes after radioembolization with resin microspheres. European Journal of Nuclear Medicine and Molecular Imaging, 2015, 42, 1202-1222.	3.3	131
20	EANM practical guidance on uncertainty analysis for molecular radiotherapy absorbed dose calculations. European Journal of Nuclear Medicine and Molecular Imaging, 2018, 45, 2456-2474.	3.3	124
21	In vivo imaging of activated microglia using [11 C]PK11195 and positron emission tomography in patients after ischemic stroke. NeuroReport, 2000, 11, 2957-2960.	0.6	121
22	Multiple Myeloma: Molecular Imaging with C-Methionine PET/CT—Initial Experience. Radiology, 2007, 242, 498-508.	3.6	105
23	Clinical relevance of imaging proliferative activity in lung nodules. European Journal of Nuclear Medicine and Molecular Imaging, 2005, 32, 525-533.	3.3	101
24	Model selection for time-activity curves: The corrected Akaike information criterion and the F-test. Zeitschrift Fur Medizinische Physik, 2009, 19, 200-206.	0.6	94
25	Breaking Chemoresistance and Radioresistance with [213Bi]anti-CD45 Antibodies in Leukemia Cells. Cancer Research, 2007, 67, 1950-1958.	0.4	93
26	188Re or 90Y-labelled anti-CD66 antibody as part of a dose-reduced conditioning regimen for patients with acute leukaemia or myelodysplastic syndrome over the age of 55: results of a phase I-II study. British Journal of Haematology, 2005, 130, 604-613.	1.2	92
27	Clinical Value of 18-Fluorine-Fluorodihydroxyphenylalanine Positron Emission Tomography/Computed Tomography in the Follow-Up of Medullary Thyroid Carcinoma. Thyroid, 2010, 20, 527-533.	2.4	78
28	Effects of Gastric Inhibitory Polypeptide on Glucose and Lipid Metabolism of Isolated Rat Adipocytes. Annals of Nutrition and Metabolism, 1988, 32, 282-288.	1.0	75
29	Molecular radiotherapy: The NUKFIT software for calculating the timeâ€integrated activity coefficient. Medical Physics, 2013, 40, 102504.	1.6	73
30	Evaluation of pyrimidine metabolising enzymes and in vitro uptake of 3'-[18F]fluoro-3'-deoxythymidine ([18F]FLT) in pancreatic cancer cell lines. European Journal of Nuclear Medicine and Molecular Imaging, 2002, 29, 1174-1181.	3.3	70
31	Imaging Bone and Soft Tissue Tumors with the Proliferation Marker [18F]Fluorodeoxythymidine. Clinical Cancer Research, 2008, 14, 2970-2977.	3.2	69
32	First Demonstration of Leukemia Imaging with the Proliferation Marker <sup>18</sup> F-Fluorodeoxythymidine. Journal of Nuclear Medicine, 2008, 49, 1756-1762.	2.8	68
33	Knowledge-based radiation therapy (KBRT) treatment planning versus planning by experts: validation of a KBRT algorithm for prostate cancer treatment planning. Radiation Oncology, 2015, 10, 111.	1.2	67
34	Early assessment of therapy response in malignant lymphoma with the thymidine analogue [18F]FLT. European Journal of Nuclear Medicine and Molecular Imaging, 2007, 34, 1775-1782.	3.3	62
35	Clinical value of 18F-fluorodihydroxyphenylalanine positron emission tomography/computed tomography (18F-DOPA PET/CT) for detecting pheochromocytoma. European Journal of Nuclear Medicine and Molecular Imaging, 2010, 37, 484-493.	3.3	62
36	Cost-Effectiveness of Hybrid PET/CT for Staging of Non–Small Cell Lung Cancer. Journal of Nuclear Medicine, 2010, 51, 1668-1675.	2.8	62

#	Article	IF	CITATIONS
37	The Effect of Total Tumor Volume on the Biologically Effective Dose to Tumor and Kidneys for <sup>177</sup> Lu-Labeled PSMA Peptides. Journal of Nuclear Medicine, 2018, 59, 929-933.	2.8	54
38	Direct comparison of [18F]FDG PET/CT with PET alone and with side-by-side PET and CT in patients with malignant melanoma. European Journal of Nuclear Medicine and Molecular Imaging, 2007, 34, 1355-1364.	3.3	53
39	Preparation and evaluation of the rhenium-188-labelled anti-NCA antigen monoclonal antibody BW 250/183 for radioimmunotherapy of leukaemia. European Journal of Nuclear Medicine and Molecular Imaging, 1999, 26, 1265-1273.	3.3	48
40	The role of patient-based treatment planning in peptide receptor radionuclide therapy. European Journal of Nuclear Medicine and Molecular Imaging, 2016, 43, 871-880.	3.3	47
41	Omission of bone scanning according to staging guidelines leads to futile therapy in non-small cell lung cancer. European Journal of Nuclear Medicine and Molecular Imaging, 2004, 31, 964-8.	3.3	46
42	Radioimmunotherapy-based conditioning for hematopoietic cell transplantation in children with malignant and nonmalignant diseases. Blood, 2011, 117, 4642-4650.	0.6	46
43	Optimized Peptide Amount and Activity for <sup>90</sup> Y-Labeled DOTATATE Therapy. Journal of Nuclear Medicine, 2016, 57, 503-508.	2.8	45
44	Treatment planning in molecular radiotherapy. Zeitschrift Fur Medizinische Physik, 2013, 23, 262-269.	0.6	44
45	Quantitative and Qualitative Assessment of Yttrium-90 PET/CT Imaging. PLoS ONE, 2014, 9, e110401.	1.1	44
46	Radioimmunotherapy with Anti-CD66 Antibody: Improving the Biodistribution Using a Physiologically Based Pharmacokinetic Model. Journal of Nuclear Medicine, 2010, 51, 484-491.	2.8	42
47	Differences in predicted and actually absorbed doses in peptide receptor radionuclide therapy. Medical Physics, 2012, 39, 5708-5717.	1.6	42
48	The NUKDOS software for treatment planning in molecular radiotherapy. Zeitschrift Fur Medizinische Physik, 2015, 25, 264-274.	0.6	41
49	Modeling and Predicting Tumor Response in Radioligand Therapy. Journal of Nuclear Medicine, 2019, 60, 65-70.	2.8	41
50	lmaging of activated microglia with PET and [11 C]PK 11195 in corticobasal degeneration. Movement Disorders, 2004, 19, 817-821.	2.2	39
51	Myeloablative Radioimmunotherapy with Re-188-anti-CD66-Antibody for Conditioning of High-Risk Leukemia Patients Prior to Stem Cell Transplantation: Biodistribution, Biokinetics and Immediate Toxicities. Cancer Biotherapy and Radiopharmaceuticals, 2002, 17, 151-163.	0.7	38
52	Cumulative radiation exposure from imaging procedures and associated lifetime cancer risk for patients with lymphoma. Scientific Reports, 2016, 6, 35181.	1.6	38
53	Targeted bone marrow irradiation in the conditioning of high-risk leukaemia prior to stem cell transplantation. European Journal of Nuclear Medicine and Molecular Imaging, 2001, 28, 807-815.	2.2	36
54	Internal radionuclide therapy: The ULMDOS software for treatment planning. Medical Physics, 2005, 32, 2399-2405.	1.6	36

#	Article	IF	CITATIONS
55	Improving Anti-CD45 Antibody Radioimmunotherapy Using a Physiologically Based Pharmacokinetic Model. Journal of Nuclear Medicine, 2009, 50, 296-302.	2.8	36
56	Lymph Node Staging in Lung Cancer Using [18F]FDG-PET. Thoracic and Cardiovascular Surgeon, 2004, 52, 96-101.	0.4	35
57	Arc therapy for total body irradiation – A robust novel treatment technique for standard treatment rooms. Radiotherapy and Oncology, 2014, 110, 553-557.	0.3	34
58	Comparison of breast simultaneous integrated boost (SIB) radiotherapy techniques. Radiation Oncology, 2015, 10, 139.	1.2	34
59	[ 18 F] 3-deoxy-3â€2-fluorothymidine positron emission tomography: alternative or diagnostic adjunct to 2-[ 18 f]-fluoro-2-deoxy- d -glucose positron emission tomography in the workup of suspicious central focal lesions?. Journal of Thoracic and Cardiovascular Surgery, 2004, 127, 1093-1099.	0.4	33
60	Partition function and force extension relation for a generalized freely jointed chain. Macromolecules, 1993, 26, 6085-6091.	2.2	32
61	Blurring of Vessels in Spiral CT Angiography: Effects of Collimation Width, Pitch, Viewing Plane, and Windowing in Maximum Intensity Projection. Journal of Computer Assisted Tomography, 1996, 20, 965-974.	0.5	32
62	Technical prerequisites and imaging protocols for CT perfusion imaging in oncology. European Journal of Radiology, 2015, 84, 2359-2367.	1.2	31
63	Investigating the Effect of Ligand Amount and Injected Therapeutic Activity: A Simulation Study for 177Lu-Labeled PSMA-Targeting Peptides. PLoS ONE, 2016, 11, e0162303.	1.1	30
64	Dependence of treatment planning accuracy in peptide receptor radionuclide therapy on the sampling schedule. EJNMMI Research, 2016, 6, 30.	1.1	29
65	The effect of ligand amount, affinity and internalization on PSMA-targeted imaging and therapy: A simulation study using a PBPK model. Scientific Reports, 2019, 9, 20041.	1.6	28
66	MITIGATE-NeoBOMB1, a Phase I/IIa Study to Evaluate Safety, Pharmacokinetics, and Preliminary Imaging of <sup>68</sup> Ga-NeoBOMB1, a Gastrin-Releasing Peptide Receptor Antagonist, in GIST Patients. Journal of Nuclear Medicine, 2020, 61, 1749-1755.	2.8	27
67	Influence of sampling schedules on [177Lu]Lu-PSMA dosimetry. EJNMMI Physics, 2020, 7, 41.	1.3	27
68	Anti-CD45 monoclonal antibody YAML568: A promising radioimmunoconjugate for targeted therapy of acute leukemia. Journal of Nuclear Medicine, 2006, 47, 1335-41.	2.8	27
69	123I-ITdU-Mediated Nanoirradiation of DNA Efficiently Induces Cell Kill in HL60 Leukemia Cells and in Doxorubicin-, Â-, or Â-Radiation-Resistant Cell Lines. Journal of Nuclear Medicine, 2007, 48, 1000-1007.	2.8	25
70	A Monte Carlo based source model for dose calculation of endovaginal TARGIT brachytherapy with INTRABEAM and a cylindrical applicator. Zeitschrift Fur Medizinische Physik, 2012, 22, 197-204.	0.6	25
71	EANM position paper on the role of radiobiology in nuclear medicine. European Journal of Nuclear Medicine and Molecular Imaging, 2021, 48, 3365-3377.	3.3	23
72	A comparison of the biodistribution and biokinetics of 99mTc-anti-CD66 mAb BW 250/183 and 99mTc-anti-CD45 mAb YTH 24.5 with regard to suitability for myeloablative radioimmunotherapy. European Journal of Nuclear Medicine and Molecular Imaging, 2003, 30, 667-673.	3.3	22

#	Article	IF	CITATIONS
73	Comparing time activity curves using the Akaike information criterion. Physics in Medicine and Biology, 2009, 54, N501-N507.	1.6	22
74	Simultaneous iterative reconstruction for emission and attenuation images in positron emission tomography. Medical Physics, 2000, 27, 2065-2071.	1.6	20
75	Simultaneous iterative reconstruction of emission and attenuation images in positron emission tomography from emission data only. Medical Physics, 2002, 29, 1962-1967.	1.6	20
76	A survey of PET activity in Germany during 1999. European Journal of Nuclear Medicine and Molecular Imaging, 2002, 29, 1091-1097.	3.3	20
77	Quantitative Imaging Of Yttrium-86 Pet with the Ecat Exact Hr+ In 2D Mode. Cancer Biotherapy and Radiopharmaceuticals, 2004, 19, 482-490.	0.7	20
78	Physiologically Based Pharmacokinetic Modeling Is Essential in 90Y-Labeled Anti-CD66 Radioimmunotherapy. PLoS ONE, 2015, 10, e0127934.	1.1	20
79	Optimal preloading in radioimmunotherapy with anti-CD45 antibody. Medical Physics, 2011, 38, 2572-2578.	1.6	19
80	Nuclear medicine dosimetry: Quantitative imaging and dose calculations. Zeitschrift Fur Medizinische Physik, 2011, 21, 246-247.	0.6	19
81	New Molecular Markers for Prostate Tumor Imaging: A Study on 2â€Methylene Substituted Fatty Acids as New AMACR Inhibitors. Chemistry - A European Journal, 2011, 17, 10144-10150.	1.7	19
82	Image-Guided Radiotherapy Using a Modified Industrial Micro-CT for Preclinical Applications. PLoS ONE, 2015, 10, e0126246.	1.1	19
83	In vivo micro-CT imaging of untreated and irradiated orthotopic glioblastoma xenografts in mice: capabilities, limitations and a comparison with bioluminescence imaging. Journal of Neuro-Oncology, 2015, 122, 245-254.	1.4	19
84	Analytical model for the microscopic nonaffine deformation of polymer networks. Journal of Chemical Physics, 1994, 101, 2532-2538.	1.2	18
85	F-18 Fluorodeoxyglucose (FDG) and C-Reactive Protein (CRP). Molecular Imaging and Biology, 1999, 2, 131-136.	0.3	18
86	Timeâ€integrated activity coefficient estimation for radionuclide therapy using PET and a pharmacokinetic model: A simulation study on the effect of sampling schedule and noise. Medical Physics, 2016, 43, 5145-5154.	1.6	18
87	Multi-Modal PET and MR Imaging in the Hen's Egg Test-Chorioallantoic Membrane (HET-CAM) Model for Initial In Vivo Testing of Target-Specific Radioligands. Cancers, 2020, 12, 1248.	1.7	18
88	Treatment of radioactive decay in pharmacokinetic modeling: Influence on parameter estimation in cardiac 13N-PET. Medical Physics, 1999, 26, 616-621.	1.6	17
89	Preferential Tumor Targeting and Selective Tumor Cell Cytotoxicity of 5-[131/1251]Iodo-4′-Thio-2′-Deoxyuridine. Clinical Cancer Research, 2008, 14, 7311-7319.	3.2	17
90	Imaging of Orthotopic Glioblastoma Xenografts in Mice Using a Clinical CT Scanner: Comparison with Micro-CT and Histology. PLoS ONE, 2016, 11, e0165994.	1.1	17

#	Article	IF	CITATIONS
91	Radioimmunotherapy for Myeloablation Before SCT in Paediatric Patients with Malignant and Non-Malignant Diseases Blood, 2007, 110, 624-624.	0.6	17
92	Potential of Optimal Preloading in Anti-CD20 Antibody Radioimmunotherapy: An Investigation Based on Pharmacokinetic Modeling. Cancer Biotherapy and Radiopharmaceuticals, 2010, 25, 279-287.	0.7	16
93	Bone marrow transplantation nephropathy after an intensified conditioning regimen with radioimmunotherapy and allogeneic stem cell transplantation. Journal of Nuclear Medicine, 2006, 47, 278-86.	2.8	16
94	[18F]5-Fluoro-2-Deoxyuridine-PET for Imaging of Malignant Tumors and for Measuring Tissue Proliferation. Cancer Biotherapy and Radiopharmaceuticals, 2003, 18, 327-337.	0.7	15
95	A fast method for rescaling voxel S values for arbitrary voxel sizes in targeted radionuclide therapy from a single Monte Carlo calculation. Medical Physics, 2013, 40, 082502.	1.6	15
96	Prediction of time-integrated activity coefficients in PRRT using simulated dynamic PET and a pharmacokinetic model. Physica Medica, 2017, 42, 298-304.	0.4	15
97	Treatment planning algorithm for peptide receptor radionuclide therapy considering multiple tumor lesions and organs at risk. Medical Physics, 2018, 45, 3516-3523.	1.6	15
98	Targeted marrow irradiation with radioactively labeled anti-CD66 monoclonal antibody prior to allogeneic stem cell transplantation for patients with leukemia: results of a phase I-II study. Haematologica, 2006, 91, 285-6.	1.7	15
99	<i>Short Communication:</i> <sup>18</sup> F-Immuno-PET: Determination of Anti-CD66 Biodistribution in a Patient with High-Risk Leukemia. Cancer Biotherapy and Radiopharmaceuticals, 2008, 23, 819-824.	0.7	14
100	Dependence of image quality on acquisition time for the PET/CT Biograph mCT. Zeitschrift Fur Medizinische Physik, 2014, 24, 73-79.	0.6	14
101	Comparison of breast sequential and simultaneous integrated boost using the biologically effective dose volume histogram (BEDVH). Radiation Oncology, 2016, 11, 16.	1.2	14
102	Validation of myocardial blood flow estimation with nitrogen-13 ammonia PET by the argon inert gas technique in humans. European Journal of Nuclear Medicine and Molecular Imaging, 2001, 28, 340-345.	2.2	13
103	Performance of Integrated FDG-PET/CT for Differentiating Benign and Malignant Lung Lesions -Results from a Large Prospective Clinical Trial. Molecular Imaging and Biology, 2008, 10, 121-128.	1.3	13
104	Comparison of five cluster validity indices performance in brain [ <sup>18</sup> F] <scp>FET</scp> â€ <scp>PET</scp> image segmentation using <i>k</i> â€means. Medical Physics, 2017, 44, 209-220.	1.6	13
105	Effect of Tumor Perfusion and Receptor Density on Tumor Control Probability in <sup>177</sup> Lu-DOTATATE Therapy: An In Silico Analysis for Standard and Optimized Treatment. Journal of Nuclear Medicine, 2021, 62, 92-98.	2.8	13
106	Iterative image reconstruction reduces apparent tumor distortion Radiology, 1997, 204, 279-279.	3.6	12
107	Treatment planning in PRRT based on simulated PET data and a PBPK model. Nuklearmedizin - NuclearMedicine, 2017, 56, 23-30.	0.3	11
108	Technical Note: Optimal sampling schedules for kidney dosimetry based on the hybrid planar/SPECT method in 177 Luâ€PSMA therapy. Medical Physics, 2019, 46, 5861-5866.	1.6	11

#	Article	IF	CITATIONS
109	Auger electron emitter against multiple myeloma — targeted endo-radio-therapy with 125I-labeled thymidine analogue 5-iodo-4′-thio-2′-deoxyuridine. Nuclear Medicine and Biology, 2011, 38, 1067-1077.	0.3	10
110	A simulation-based method to determine optimal sampling schedules for dosimetry in radioligand therapy. Zeitschrift Fur Medizinische Physik, 2019, 29, 314-325.	0.6	10
111	Important pharmacokinetic parameters for individualization of <sup>177</sup> Luâ€PSMA therapy: A global sensitivity analysis for a physiologicallyâ€based pharmacokinetic model. Medical Physics, 2021, 48, 556-568.	1.6	10
112	Comparison of Quantification of Target-Specific Accumulation of [18F]F-siPSMA-14 in the HET-CAM Model and in Mice Using PET/MRI. Cancers, 2021, 13, 4007.	1.7	10
113	A population-based method to determine the time-integrated activity in molecular radiotherapy. EJNMMI Physics, 2021, 8, 82.	1.3	10
114	Microscopic Nonaffine Deformation of Polydisperse Polymer Networks. Macromolecules, 1995, 28, 5906-5909.	2.2	9
115	Investigation of the imaging characteristics of the ALBIRA II small animal PET system for 18 F, 68 Ga and 64 Cu. Zeitschrift Fur Medizinische Physik, 2017, 27, 132-144.	0.6	9
116	A Physiologically Based Pharmacokinetic Model for In Vivo Alpha Particle Generators Targeting Neuroendocrine Tumors in Mice. Pharmaceutics, 2021, 13, 2132.	2.0	9
117	Endogenous Opiates Do Not Influence Glucose and Lipid Metabolism in Rat Adipocytes. Experimental and Clinical Endocrinology and Diabetes, 1988, 91, 350-354.	0.6	8
118	Freely jointed chain with variable segment number and length. Colloid and Polymer Science, 1995, 273, 32-37.	1.0	8
119	ROC analysis for assessment of lesion detection performance in 3D PET: Influence of reconstruction algorithms. Medical Physics, 2003, 30, 2315-2319.	1.6	8
120	Sensitivity Analysis of a Physiologically Based Pharmacokinetic Model Used for Treatment Planning in Peptide Receptor Radionuclide Therapy. Cancer Biotherapy and Radiopharmaceuticals, 2016, 31, 217-224.	0.7	8
121	Quantification of 18F-FDG uptake in non-small cell lung cancer: a feasible prognostic marker?. Journal of Nuclear Medicine, 2004, 45, 1274-6.	2.8	8
122	Are the continuum and the lattice representation of freely jointed chains equivalent?. Macromolecular Theory and Simulations, 1994, 3, 575-583.	0.6	7
123	Dependence of the anti-CD66 antibody biodistribution on the dissociation constant: A simulation study. Zeitschrift Fur Medizinische Physik, 2011, 21, 301-304.	0.6	7
124	Analysing saturable antibody binding based on serum data and pharmacokinetic modelling. Physics in Medicine and Biology, 2011, 56, 73-86.	1.6	7
125	<sup>19</sup> F Oximetry with semifluorinated alkanes. Artificial Cells, Nanomedicine and Biotechnology, 2016, 44, 1861-1866.	1.9	7
126	Quantitative analysis of regional distribution of tau pathology with 11C-PBB3-PET in a clinical setting. PLoS ONE, 2022, 17, e0266906.	1.1	7

#	Article	IF	CITATIONS
127	Improving binding potential analysis in [11C]raclopride PET studies using cluster analysis. Medical Physics, 2004, 31, 902-906.	1.6	6
128	Modelling radioimmunotherapy with anti-CD45 antibody to obtain a more favourable biodistribution. Nuklearmedizin - NuclearMedicine, 2009, 48, 113-119.	0.3	6
129	Population-Based Modeling Improves Treatment Planning Before 90Y-Labeled Anti-CD66 Antibody Radioimmunotherapy. Cancer Biotherapy and Radiopharmaceuticals, 2015, 30, 285-290.	0.7	6
130	Modelling the internalisation process of prostate cancer cells for PSMA-specific ligands. Nuclear Medicine and Biology, 2019, 72-73, 20-25.	0.3	6
131	Effect of vasoactive intestinal polypeptide (VIP) on glucose and lipid metabolism of isolated rat adipocytes. Research in Experimental Medicine, 1988, 188, 189-195.	0.7	5
132	Iterative reconstruction for attenuation correction in positron emission tomography: Maximum likelihood for transmission and blank scan. Medical Physics, 1999, 26, 1838-1842.	1.6	5
133	Determination of individual organ masses for 90Y-anti-CD66 radioimmunotherapy: Influence on therapy planning. Zeitschrift Fur Medizinische Physik, 2011, 21, 305-309.	0.6	5
134	Mathematical Modeling of In Vivo Alpha Particle Generators and Chelator Stability. Cancer Biotherapy and Radiopharmaceuticals, 2021, , .	0.7	5
135	Determination of the Immunoreactivity of Radiolabeled Monoclonal Antibodies: A Theoretical Analysis. Cancer Biotherapy and Radiopharmaceuticals, 2006, 21, 15-21.	0.7	4
136	Radiation-induced malignancies after intensity-modulated versus conventional mediastinal radiotherapy in a small animal model. Scientific Reports, 2019, 9, 15489.	1.6	4
137	Quantitative Imaging of Yttrium-86 PET with the ECAT EXACT HR <sup>+</sup> in 2D Mode. Cancer Biotherapy and Radiopharmaceuticals, 2004, 19, 482-490.	0.7	4
138	Pathophysiological Basis and Clinical Value of <sup>18</sup> F-Fluorodeoxyglucose and Positron Emission Tomography in Pancreatic Adenocarcinoma. Digestive Surgery, 1994, 11, 360-365.	0.6	3
139	Functionality dependence for molecular nonaffine deformation of polymer networks. Polymer, 1997, 38, 4049-4052.	1.8	3
140	Quantitative image reconstruction in PET from emission data only using cluster analysis. Zeitschrift Fur Medizinische Physik, 2003, 13, 269-274.	0.6	3
141	A Method for Point Spread Function Estimation for Accurate Quantitative Imaging. IEEE Transactions on Nuclear Science, 2018, 65, 961-969.	1.2	3
142	A single-source photon source model of a linear accelerator for Monte Carlo dose calculation. PLoS ONE, 2017, 12, e0183486.	1.1	3
143	Physiologically based pharmacokinetic modeling of 18F-SiFAlin-Asp3-PEG1-TATE in AR42J tumor bearing mice. Nuclear Medicine and Biology, 2016, 43, 243-246.	0.3	2
144	Collimator optimization for small animal radiation therapy at a micro-CT. Zeitschrift Fur Medizinische Physik, 2017, 27, 56-64.	0.6	2

#	Article	IF	CITATIONS
145	Focus on the Low-Dose Bath: No Increased Cancer Risk After Mediastinal VMAT Versus AP/PA Irradiation in a Tumor-Prone Rat Model. International Journal of Radiation Oncology Biology Physics, 2017, 99, S76-S77.	0.4	2
146	Performance assessment of the ALBIRA II pre-clinical SPECT S102 system for 99mTc imaging. Annals of Nuclear Medicine, 2021, 35, 111-120.	1.2	2
147	A knowledgeâ€based quantitative approach to characterize treatment plan quality: Application to prostate VMAT planning. Medical Physics, 2021, 48, 94-104.	1.6	2
148	A Whole-Body Physiologically Based Pharmacokinetic Model for Alpha Particle Emitting Bismuth in Rats. Cancer Biotherapy and Radiopharmaceuticals, 2021, , .	0.7	2
149	2â€(fluorineâ€18)fluoroâ€2â€deoxyâ€Dâ€glucose positron emission tomography in the detection and staging of malignant lymphoma. Cancer, 2001, 91, 889-899.	2.0	2
150	Combined stereotactic biopsy and stepping-source interstitial irradiation of glioblastoma multiforme. Journal of Neurosurgical Sciences, 2018, 62, 214-220.	0.3	2
151	Influence of microscopic nonâ€ <b>e</b> ffinity and functionality on the deformation of polymeric networks. Macromolecular Symposia, 1994, 81, 129-137.	0.4	1
152	Polymer chains with correlations between adjacent segments: Qualitative differences to the freely jointed chain. Journal of Chemical Physics, 1995, 102, 3448-3451.	1.2	1
153	Towards to hENT1-nucleoside transporter selective imaging agents. Synthesis and in vitro evaluation of the radiolabeled SAENTA analogues. Bioorganic and Medicinal Chemistry Letters, 2009, 19, 5151-5154.	1.0	1
154	Converting a Standard Micro-CT Into an IGRT-Competent Small Animal Irradiation Device. International Journal of Radiation Oncology Biology Physics, 2014, 90, S804-S805.	0.4	1
155	Modeling sphere dynamics in blood vessels for SIRT pre-planning – To fathom the potential and limitations. Zeitschrift Fur Medizinische Physik, 2019, 29, 5-15.	0.6	1
156	Comparison of MRI-based and PET-based image pre-processing for quantification of 11C-PBB3 uptake in human brain. Zeitschrift Fur Medizinische Physik, 2021, 31, 37-47.	0.6	1
157	The HIV-derived protein Vpr52-96 has anti-glioma activity in vitro and in vivo. Oncotarget, 2016, 7, 45500-45512.	0.8	1
158	Dynamical Cluster Analysis for the Detection of Microglia Activation. , 2001, , 442-445.		1
159	Radiosynthesis and evaluation of [11C]BTA-1 and [11C]3'-Me-BTA-1 as potential radiotracers for in vivo imaging of-amyloid plaques. Nuklearmedizin - NuclearMedicine, 2007, , .	0.3	1
160	An in silico study on the effect of the radionuclide half-life on PET/CT imaging with PSMA-targeting radioligands. Nuklearmedizin - NuclearMedicine, 2021, 60, 33-37.	0.3	1
161	Breast Radiation Therapy (RT) Using Simultaneous Integrated Boost (SIB): Which Is the Optimal Intensity Modulated RT (IMRT) Technique?. International Journal of Radiation Oncology Biology Physics, 2014, 90, S227-S228.	0.4	0
162	Intraoperative radiation therapy. Zeitschrift Fur Medizinische Physik, 2014, 24, 1-2.	0.6	0

#	Article	IF	CITATIONS
163	Comparison of Knowledge Based Radiation Therapy Treatment Plans Against Expert Plans for Prostate VMAT. International Journal of Radiation Oncology Biology Physics, 2015, 93, E582.	0.4	0
164	Comparison of Breast Sequential and Simultaneous Integrated Boost Using the Biologically Effective Dose Volume Histogram (BEDVH). International Journal of Radiation Oncology Biology Physics, 2015, 93, E14-E15.	0.4	0
165	The HIV-Derived Protein Vpr52-96 Has Antiglioma Activity In Vitro and In Vivo. International Journal of Radiation Oncology Biology Physics, 2015, 93, S141-S142.	0.4	0
166	Session 2. Cells, materials and biochemistry I. Biomedizinische Technik, 2017, 62, .	0.9	0
167	[OA142] Validation framework for automated determination of the optimal number of clusters in [F-18]FET-PET brain images. Physica Medica, 2018, 52, 54.	0.4	0
168	Changes in Eosinophil as potential marker for immune-related changes associated with PRRT in NET. Nuklearmedizin - NuclearMedicine, 2021, 60, .	0.3	0
169	Chaotic Motion of Molecular Chains. NATO ASI Series Series B: Physics, 1991, , 195-214.	0.2	0
170	Abstract 4458: The HIV-derived protein Vpr52-96has anti-glioma activity in vitro and in vivo. , 2015, , .		0
171	Physikalisch-technische Grundlagen und Tracerentwicklung in der Positronenemissionstomografie. , 2017, , 19-56.		0
172	Radiation Dosimetry in Ibritumomab Therapy. Resistance To Targeted Anti-cancer Therapeutics, 2018, , 105-117.	0.1	0